This paper appears in the Journal of Medical Robotics Research, 2018.
DOI: 10.1142/S2424905X18410039

Journal of Medical Robotics Research, Vol. 0, No. 0 (2017) 1–15

Switched-Impedance Control of Surgical Robots in Teleoperated Beating-Heart Surgery

Lingbo Cheng, Mahdi Tavakoli

Department of Electrical and Computer Engineering, University of Alberta, Edmonton, AB, T6G 2V4, Canada
E-mail: lingbo1@ualberta.ca , mahdi.tavakoli@ualberta.ca

A novel switched-impedance control method is proposed and implemented for telerobotic beating-heart surgery. Differing from cardiopulmonary-bypass-based arrested-heart surgery, beating-heart surgery creates challenges for the human operator (surgeon) due to the heart's fast motions and, in the case of a teleoperated surgical robot, the oscillatory haptic feedback to the operator. This paper designs two switched reference impedance models for the master and slave robots to achieve both motion compensation and non-oscillatory force feedback during slave-heart interaction. By changing the parameters of the impedance models, different performances for both robots are obtained: (a) when the slave robot does not make contact with the beating heart, the slave robot closely follows the motion of the master robot as in a regular teleoperation system, (b) when contact occurs, the slave robot automatically compensates for the fast motions of the beating heart while the human operator perceives the non-oscillatory component of the slave-heart interaction forces, creating the feeling of making contact with an idle heart for the human operator. The proposed method is validated through simulations and experiments.

Keywords: Beating-heart surgery; teleoperation; motion compensation; non-oscillatory haptic feedback.

1. Introduction

Telerobotics-assisted surgeries are becoming increasingly common due to their enhanced accuracy and the convenience of manipulating a master robot to command a slave robot to perform surgeries. Telerobotics assistance can be used to enable and improve the performance of beating-heart surgery.

Different from arrested-heart surgery that may result in negative side effects including neurologic dysfunction in adults, delayed neural development in children, and even damages in the major vessels [1]–[3], beating-heart surgery enables intraoperative evaluation of the heart motion while eliminating the above negative effects. However, the rapid motions of the beating heart and the poor quality of the force feedback to the human operator create challenges that can be addressed through teleoperated beating-heart surgery. In essence, to minimize the risk of tool-tissue collision and tissue injury and ensure the haptic feedback to the operator precludes oscillatory tool-tissue interaction forces, the slave robot should have compliance with respect to the beating heart's motion. If the slave robot can move the surgical tool in synchrony with the beating heart's motion, the oscillatory forces of the slave-heart contact will be negligible, and the human operator will have the haptic feeling of making contact with an arrested heart.

Various configurations of robot-assisted beating-heart surgical systems have been presented before. Using sonomicrometry crystals to track the beating heart motion in real time and generalized adaptive predictors to predict the heart's motion, motion compensation systems have been reported in [4]–[6]. Riviere *et al.* [7] and Ginhoux *et al.* [8] used a high-speed camera to track optical markers and LEDs attached to a beating porcine heart, respectively, to assess the motion of the heart. These sensors achieved perfect performance in heart motion compensation. High-speed cameras, however, are not appropriate for interior heart surgeries. In addition, the utilization of 3D ultrasound images to track the beating heart tissue in real time as a basis for synchronizing the surgical tool with the fast moving cardiac tissue has been reported in [9]–[12]. Much of the past work, however, used a hand-held device for surgery instead of utilizing a teleoperation system. A teleoperation system provides the advantage of enabling the human operator to interact with environments that are inaccessible or confined (such as in minimally invasive surgery) from an ergonomic console. Thus, our research group developed a telerobotics-based solution for beating-heart surgery by various filters and controllers that use ultrasound images to track and estimate the motion of the beating heart [13]–[17]. However, the lack of haptic feedback for the human operator makes the surgical operations difficult [18].

Haptic feedback during operation is important for human operator to be able to accurately execute the surgical tasks especially in beating heart surgeries involving tissue cutting and sewing, dissection, grasping, and so on [18]–[21]. During the operation of such surgical tasks, the heart tissue undergoes a physically damaging process, which requires the tool-tissue

interaction force to be within a safety range to avoid potential tissue injury.

To precisely apply forces to the beating heart and incorporate haptic feedback to the human operator, some other methods involving force control strategies were proposed. Bebek et al. proposed motion tracking strategy by utilizing a force-based model predictive controller [22]. Kesner et al. designed controllers on the basis of an inner position loop where the position trajectory was adjusted to achieve a desired force on the heart [23], [24]. To ensure the safety and accuracy of force tracking, Yuen et al. [25] designed a force controller incorporating a feed-forward term containing the estimated motion of the beating heart. In addition, Nakajima et al. [26] performed haptic feedback and motion compensation by using acceleration-based bilateral control and visual servoing. However, all of these methods still need vision/imaging sensors to estimate the position the beating heart. This results in inevitable practical limitations such as large time delays (due to acquiring and processing image data), low sampling rates (due to low frame rates of imagers), uncertainty due to visual occlusions, etc.

To get around the limitations of visual sensors, some researchers developed force feedback teleoperation systems [27]–[32] and/or designed miniature force sensors used in microsurgeries [33]. Specifically, Moreira *et al*. [28], [29] proposed a force control method using a viscoelastic active observer to compensate for the physiological motion. In addition, Dominici and Cortesao achieved beating-heart motion compensation by designing a cascade model predictive control architecture with a Kalman active observer [30], [31], and a double active observer architecture [32]. All of these methods were using pure force control with active observer to cope with beating heart motion. Also, in the case of pure force control, it is assumed that the slave robot has somehow been initially controlled to come into contact with the heart tissue, and its goal is maintaining contact between the tool and the tissue. Therefore, for the non-contact case and the requirement of performing a surgical task such as tissue penetrating, the pure force control may be not applicable.

In this paper, we present a switched impedance-controlled teleoperation system to achieve two objectives in noncontact and contact situations as far as interaction between the slave robot and the beating heart is concerned. In our developed system, a thin rigid surgical tool is mounted on the end of the slave robot, where a force sensor attached. Considering the volume of the force sensor, in realistic surgery the thin and long surgical tool will be inserted into the heart through a suture on the exterior heart wall, and leave the force sensor outside the body. By utilizing the measured interaction forces and without any need for vision-based (image-based) heart motion estimation, active observer and/or motion prediction, the following two desired behaviors for the master and slave robots can be achieved.

First, when there is no contact between the slave robot and the heart tissue, the slave robot precisely mimics the motion of the master robot, which is being manipulated by the human operator. It should be noted that compared to the fast motion of the beating heart, the motion of the human operator/master robot has a relatively low frequency. Second, when contact occurs, the slave robot compensates for the fast movements of the beating heart while at the same time following the commands of the human operator. In other words, as the slave robot followed the human operator's motions, it also synchronizes its motion to that of the beating heart. Based on that, the slave-heart interaction force mainly caused by the motion of slave robot has two frequency components. As far as the force feedback about the slave-heart interaction to the human operator is concerned, there is a need to only reflect the low-frequency component of slave-heart interaction force which is caused by the motion of human operator; the high-frequency component of it is due to any residual mismatch between the heart motion and the slave robot motion, and also due to the internal inertia of the force sensor (which makes it register a sinusoidal force when the sensor undergoes an oscillatory motion even under no contact). Therefore, this teleoperation system guarantees that the slave robot both implements rapid compensation for the beating heart's motion and executes the commands of the human operator to perform a given task on or inside the heart. In this way, the operator does not need to synchronize the master robot's motion with the moving heart's motion manually, which would have been a daunting task. The above objectives can be achieved by properly choosing the parameters of the reference impedance models for the master and slave robots.

The rest of this paper is organized as follows. Section 2 introduces the switched impedance-controlled telerobotic system including the developed system architecture, reference impedance models, adjustment guidelines for the model parameters, and controllers used in the system. Section 3 describes the validation protocol. Section 4 and 5 present the simulation and experimental results, respectively. Finally, the concluding remarks are given in Section 6.

2. Switched Impedance-Controlled Teleoperation System

2.1. *Telerobotic system*

A teleoperated beating-heart surgery system includes four pieces (Fig. 1): the human operator, the master robot, the slave robot, and the beating heart. The human operator manipulates the master robot. The slave robot follows the motions of the human operator to implement specific maneuvers related to a given task on the beating heart.

By using the developed telerobotic system, the desired position-tracking performance is shown in the left part of the ideal behavior block. To graphically identify the noncontact

and contact cases, the heart's position (dotted green line) is shown to have an offset from the initial positions of the master (solid red line) and slave (dashed blue line) robots' end-effectors. When the dotted green line is above the latter two lines, it means there is no contact, and the master and the slave have the same trajectory; otherwise, contact has been made, and the slave robot is to follow the master's commands *and* compensates for the heart's oscillatory motion. The desired force performance is shown in the right part of the ideal behavior block. When there is no contact, the slave-heart interaction force (dashed red line) stays at zero; while when contact, it should be similar to the human-master interaction force (solid black line).

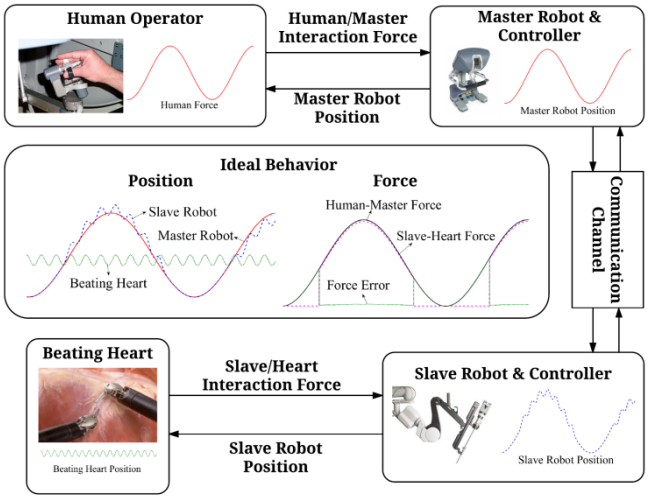

Fig.1. The telerobotic system and ideal behaviors of position and force for beating heart surgery. The left and right parts of the ideal behavior block show the desired position-tracking performance and the desired force performance, respectively.

Teleoperated beating-heart surgery involves two phases: No contact with the heart and contact with the heart as far as the slave robot is concerned. Contact detection can be achieved based on the slave-tissue interaction force, which can be measured by a force sensor mounted on the end-effector of the slave robot. Theoretically, if the slave-tissue interaction force equals zero, the slave robot has not made contact with the heart; otherwise, it has.

When there is no contact between the beating heart and the slave robot, which happens when the human operator is either not doing anything or trying to manipulate the master robot such that the slave robot gets closer to or farther from the heart surface, the slave robot should simply follow the (possibly scaled) trajectory of the master robot.

When the slave robot is in contact with the beating heart, there are two requirements. First, to avoid the induced motion phenomenon [34], the human operator should only feel what one would feel when directly working on an arrested heart. This means the quasi-periodic heartbeat-induced forces caused by the residual mismatch between the robot and the heart motions and by the slave-mounted force sensor's internal inertia should not be transmitted to the operator. Second, the slave robot should synchronize its motions with the heart's motion *and* follow the commands of the human operator as closely as possible to execute the desired surgical task.

To achieve the desired behaviors described in Fig. 1, the detailed model developments, parameter tuning, and controller design are presented below. Transmitting the force and position information of the master and slave robots through the communication channel, two reference impedance models for the master and slave robots are proposed. The reference impedance models generate reference positions for the two robots, which are then sent to the master and slave position controllers (Fig. 2).

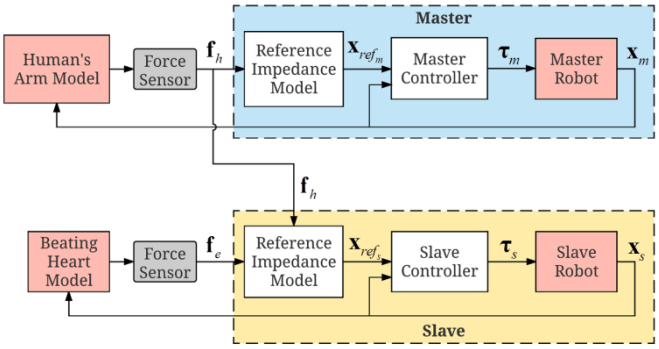

Fig.2. The block diagram of the teleoperated control system with master and slave reference impedance models.

In Fig. 2, $\mathbf{f}_h$ is the interaction force between the master and the operator, and $\mathbf{f}_e$ is the interaction force between the slave and the beating heart. They are measured directly through two force sensors. Also, $\mathbf{x}_{ref_m}$ and $\mathbf{x}_{ref_s}$ are the desired positions for the master and slave robots, which are generated by the reference impedance models for the respective robot. Note that $\mathbf{x}_m$ and $\mathbf{x}_s$ are the actual positions of the master and slave robots, respectively. The controllers receive the position errors between the desired positions generated by the reference models and the actual positions read from the robots, and then output torques $\boldsymbol{\tau}_m$ and $\boldsymbol{\tau}_s$ to the robots. The position of the beating heart is indicated by $\mathbf{x}_e$. The initial point of beating heart position is set when the slave robot is far away from the heart, and meanwhile the heart is closest to the slave robot.

In this paper, communication delay is not considered because long-distance telesurgery of the beating heart is not the goal. The purpose of the telerobotics-assisted surgical system is to enable motion compensation and non-oscillatory haptic feedback during beating-heart surgery while allowing the human operator to operate from a user console.

2.2. *Reference impedance models for the robots*

This section presents two appropriate reference impedance models for the master and slave robots, respectively. The reference impedance model of the master robot expresses a dynamical relationship between the operator-master interaction force and the difference between the master impedance model's response (which is the desired position for the master robot) and a varying initial trajectory as

$$m_m\ddot{\mathbf{x}}_{ref_m} + c_m\dot{\mathbf{x}}_{ref_m} + k_m\tilde{\mathbf{x}}_{ref_m} = \mathbf{f}_h$$
$$\tilde{\mathbf{x}}_{ref_m} = \mathbf{x}_{ref_m} - \mathbf{x}_{ini_m}, \text{ where } \begin{cases} \mathbf{x}_{ini_m} = 0, & \text{when } \mathbf{f}_e = 0 \\ \mathbf{x}_{ini_m} = \mathbf{x}_{m_0}, & \text{when } \mathbf{f}_e \neq 0 \end{cases} \quad (1)$$

In the above, m_m, c_m, k_m are the mass, damping and virtual stiffness parameters of the master impedance model. Also, $\mathbf{x}_{ini_m}$ is the initial position for the master robot. When there is no contact between the slave robot and the tissue ($\mathbf{f}_e = 0$), $\mathbf{x}_{ini_m}$ equals 0; when contact occurs ($\mathbf{f}_e \neq 0$), $\mathbf{x}_{ini_m}$ is chosen to be $\mathbf{x}_{m_0}$, which is the master robot position when the slave robot first makes contact with the beating heart. $\mathbf{x}_{ini_m}$ is set according to the above to ensure $\mathbf{x}_m$ continuously increase during the transition between noncontact and contact cases, as the impedance parameters of model (1) will be changed according to the absence or presence of contact.

The reference impedance model for the slave robot is defined as a dynamical relationship between a force summation (involving the scaled human-master interaction force and the slave-heart interaction force) and the difference between the slave impedance model's response and a varying initial trajectory as

$$m_s\ddot{\mathbf{x}}_{ref_s} + c_s\dot{\mathbf{x}}_{ref_s} + k_s\tilde{\mathbf{x}}_{ref_s} = k_f\mathbf{f}_h - \mathbf{f}_e$$
$$\tilde{\mathbf{x}}_{ref_s} = \mathbf{x}_{ref_s} - \mathbf{x}_{ini_s}, \text{ where } \begin{cases} \mathbf{x}_{ini_s} = 0, & \text{when } \mathbf{f}_e = 0 \\ \mathbf{x}_{ini_s} = \mathbf{x}_{s_0}, & \text{when } \mathbf{f}_e \neq 0 \end{cases} \quad (2)$$

Here, k_f is a force scaling factor, and m_s, c_s, k_s are the mass, damping and virtual stiffness parameters of the slave impedance model. Similar to $\mathbf{x}_{ini_m}$, the initial position $\mathbf{x}_{ini_s}$ should be reset as the parameters of the slave impedance model will be changed depending on the absence or presence of contact. Also, $\mathbf{x}_{s_0}$ is the slave robot's position when the slave robot first contacts the beating heart.

The reference impedance models for the master and slave robots are stable second-order differential equations when the impedance parameters are set to be positive. The stability characteristic of reference impedance models enhances the patient safety during the robot-assisted surgery.

To achieve motion compensation and non-oscillatory force feedback during slave-heart interaction, the parameters for the two impedance models should be adjusted appropriately. Instead of tuning all of these parameters directly, damping ratios and natural frequencies of the models are used to adjust the impedance models.

The damping ratios of the two models can be expressed as $\zeta_m = c_m/2\sqrt{m_m k_m}$ and $\zeta_s = c_s/2\sqrt{m_s k_s}$, which describe how oscillations decay after an input. In order to ensure the impedance model (1) and (2) have fast behaviors in response to the force inputs and small overshoots in response to the step force inputs, the damping ratios are both set as 0.7.

The natural frequencies (the cut-off frequency for damping ratio equals 0.7) of the two impedance models are given by $\omega_{n_m} = \sqrt{k_m/m_m}$ and $\omega_{n_s} = \sqrt{k_s/m_s}$. For the purpose of disturbance rejection and compliance with heart's motion, different ω_{n_m} and ω_{n_s} should be chosen according to the absence or presence of contact between the slave robot and the heart. In addition, the stiffness values of the two models k_m and k_s need to be designed first, so that the mass and damping parameters can be obtained from the natural frequencies and the damping ratios. Therefore, the parameters need to be adjusted below are only stiffness and natural frequency.

2.3. *Adjustment of impedance models for no contact case*

For the case of no contact, the slave robot should follow the (possibly scaled) trajectory of the master robot. To achieve this objective, the parameters of the two impedance models for the master and slave robots should be proportional to one another (i.e., $k_{m1} = k_p k_{s1}$, $\zeta_{m1} = \zeta_{s1}$, $\omega_{n_{m1}} = \omega_{n_{s1}}$), which will lead to a scaled position tracking ($\mathbf{x}_{ref_{m1}} = k_p\mathbf{x}_{ref_{s1}}$). Here, k_p is a position scaling factor, which equals $1/k_f$ and can be set to unity for simplicity.

In reality, when there is no contact, the human operator should only sense the master robot's dynamics and should be able to perceive the switch between noncontact and contact. To realize these, for the noncontact case, both the master and the slave impedances are chosen to be very small (Known damping ratio and natural frequency, $k_{m1} = k_{s1} \approx 0$).

Moreover, for the purpose of avoiding the uncontrollable hand tremor of the human operator (ω_t = 6 ~ 12 Hz = 37.68 ~ 75.36 rad/sec), and taking the low-frequency motion of the human hand (ω_o = 0.05 ~ 0.2 rad/sec) into consideration, the natural frequencies are designed to be chosen within a small range (i.e. $10\omega_o \leq \omega_{n_{m1}} (= \omega_{n_{s1}}) \leq 0.1\omega_t$). Consequently, in the following section, when there is no contact, $\omega_{n_{m1}}$ and $\omega_{n_{s1}}$ are set to be 1 rad/sec.

2.4. *Adjustment of impedance models for contact case*

When the slave robot makes contact with the beating heart tissue, the human operator's force affects both the master and the slave impedance models.

In the slave impedance model (2), to guarantee the scaled human-master interaction force to be as similar as the slave-heart interaction force, the impedance for the slave robot should be adjusted to be very small (i.e., $k_{s2} \approx 0$). Then the left side of (2) becomes small due to the boundedness of $\mathbf{x}_{ref_{s2}}$, $\dot{\mathbf{x}}_{ref_{s2}}$ and $\ddot{\mathbf{x}}_{ref_{s2}}$, and accordingly, the right side of this equation will be small as well ($(k_f\mathbf{f}_h - \mathbf{f}_e) \rightarrow 0$). Therefore, position tracking of the slave robot can be attained. In other words, the slave robot will compensate for the heart's motion and follow the scaled position of the master robot ($(\mathbf{X}_s \rightarrow (k_f Z_{m2}/Z_e)\mathbf{X}_m + \mathbf{X}_e)$, where $\mathbf{X}$ is the Laplace transform of the position, Z_{m2} and Z_e are the impedances of the master model and the heart), as $(k_f\mathbf{F}_h - \mathbf{F}_e) = (k_f Z_{m2}\mathbf{X}_{ref_{m2}} - Z_e(\mathbf{X}_s - \mathbf{X}_e)) \rightarrow 0$.

Furthermore, the slave impedance model (2) should comply with the slave-heart interaction force. Therefore, the natural frequency is selected several times greater than the range of beating heart frequency ($\omega_{n_{s2}} \gg \omega_h$ (= 6.28 ~ 10.68 rad/sec)). Particularly, $\omega_{n_{s2}}$ is set to be 50 rad/sec.

In the master impedance model (1), the natural frequency is set to be the same as that for the noncontact case ($\omega_{n_{m2}}$= 1 rad/sec) to filter the high-frequency component. Therefore, the only varying parameter of the master impedance model is the stiffness (k_{m2}). As the slave-heart interaction force is approximately equal to the scaled human-master interaction force, the human operator should exert appropriate forces to the slave impedance model (2). For this purpose, k_{m2} should be adjusted appropriately. If it is set to be a very small value, in order to apply a desired force to the slave robot, the human operator has to move the master robot through a large distance, which may be beyond the workspace for the master robot. On the contrary, if k_{m2} is chosen to be very large, the master robot will become too rigid to be manipulated; that is, a tiny movement of the master robot will generate a pretty large force.

Based on that, generally, k_{m2} can be set to be the same as the stiffness of the tissue target (k_e), so that the human operator will have the sense of directly operating on the environment – specifically, a seemingly "arrested" heart. The slave robot will follow the trajectories of the master robot and the heart ($\mathbf{x}_s \rightarrow k_f\mathbf{x}_m + \mathbf{x}_e$), as $Z_{m2} \approx Z_e$. Nevertheless, if the stiffness of the tissue target cannot be measured in advance, k_{m2} can be chosen from the range of the stiffness for soft organs, 100-300 N/m [35], [36]. By tuning the force scaling factor, k_f, the force applied by the human operator to the slave impedance model (2) can be adjusted to the desired range.

It is reasonable to tune the force scaling factor instead of the workspace of the master robot to adjust the applied force to the slave robot, as for cases that require small slave-heart interaction forces the force scaling factor can reduce the tissue injury caused by accident.

2.5. *Switch of impedance models*

According to the absence or presence of contact between the slave robot and the heart, the objectives and parameter adjustment guidelines for the impedance models are summarized in Table 1.

Table.1. Objectives and parameter adjustment guidelines for the two impedance models

Condition	**No contact**		**Contact**	
	Master	**Slave**	**Master**	**Slave**
Objective	$\mathbf{f}_h \approx 0$, $\mathbf{x}_m = \mathbf{x}_s$		$\mathbf{x}_s \approx k_f\mathbf{x}_m + \mathbf{x}_e$, $k_f\mathbf{f}_h = \mathbf{f}_e$	
Stiffness	$k_{m1} = k_{s1} \approx 0$ To simulate master robot's dynamics		$k_{m2} \approx k_e$ To provide sense of operating on an idle heart	$k_{m1} = k_{s1} \approx 0$ To simulate master robot's dynamics
Natural Frequency (rad/sed)	$\omega_{n_{m1}} = \omega_{n_{s1}} = \omega_{n_{m2}} = \omega_{n_{s2}} = 1$ To reduce hand tremor and comply with the force $\mathbf{f}_h$			$\omega_{n_{s2}} = 50$ To comply with the force $\mathbf{f}_e$
Damping ratio	$\zeta_{m1} = \zeta_{s1} = \zeta_{m2} = \zeta_{s2} = 0.7$ To ensure model (1) and (2) have fast behaviors in response to the force inputs and small overshoots in response to the step force inputs			
Mass and damping	Calculate from $\omega_{n_m} = \sqrt{k_m/m_m}$, $\zeta_m = c_m/2\sqrt{m_m k_m}$, and $\omega_{n_s} = \sqrt{k_s/m_s}$, $\zeta_s = c_s/2\sqrt{m_s k_s}$			

2.6. *Controllers for impedance responses tracking*

To track the ideal responses of the two reference impedance models for the master and slave robots, two proportional-integral-derivative controllers (PID controllers) are employed and tuned based on the dynamics of the master and slave robots. These position controllers make sure the master and slave robots track the desired positions calculated from the reference impedance models for the respective robots, which are given in (1) and (2), respectively. In Fig. 2, the control variables $\boldsymbol{\tau}_m(t)$ and $\boldsymbol{\tau}_s(t)$ are determined by two weighted sums:

$$\boldsymbol{\tau}_m(t) = K_{p_m}\mathbf{e}_m(t) + K_{i_m}\int_0^t \mathbf{e}_m(\tau)d\tau + K_{d_m}\frac{d\mathbf{e}_m(t)}{dt} \quad (3)$$

$$\boldsymbol{\tau}_s(t) = K_{p_s}\mathbf{e}_s(t) + K_{i_s}\int_0^t \mathbf{e}_s(\tau)d\tau + K_{d_s}\frac{d\mathbf{e}_s(t)}{dt} \quad (4)$$

where $\mathbf{e}_i(t) = \mathbf{x}_{imp_i}(t) - \mathbf{x}_i(t)$. Here, the subscript $i = m$ for the master and $i = s$ for the slave. Also, K_{p_i}, K_{i_i} and K_{d_i}, all non-negative values, denote the coefficients for the proportional, integral, and derivative terms, respectively.

3. Testing Protocol

To validate the proposed telerobotic framework, two scenarios amenable to two surgical tasks including mitral valve annuloplasty (MVA) [19], and soft tissue cutting (STC) [20], [21] are tested in both simulations and experiments. A user study involving a line drawing task, which is similar to tissue cutting, is conducted in experiments.

3.1. *Surgical tasks*

The two surgical tasks considered in this paper require different tool-tissue contact forces. Based on this, the two scenarios are designed to achieve the desired contact forces of the tasks by tuning the model parameters. The requirements of contact forces for specific surgical tasks are described below.

In mitral valve annuloplasty, the surgical tool should compensate for the heart's fast motions to allow the human operator to easily deploy anchors into the moving annulus. In [19], Yuen provided the required contact forces of 2~3 N to deploy anchors firmly into the annulus, and emphasized that forces must stay below 5.5 N to avoid tissue damage.

In soft tissue cutting, the maximum cutting force indicates the required force for the blade to cut into the tissue. The authors in [20] and [21] studied the tissue cutting process of excised organs and showed the cutting force increased linearly in terms of magnitude as the tissue deformed; the cutting force peak was found to be greater than 3~4 N.

3.2. *Protocol*

To apply appropriate forces to the target tissue during surgery and avoid tissue damage, a simple way allowed by (2) in the proposed framework is to roughly fix the master-human interaction force, $\mathbf{f}_h$, and tune the force scaling factor, k_f. For instance, if $\mathbf{f}_h$ is around 3~4 N, the force scaling factor for the two aforementioned tasks can be set at 0.63, and 1, respectively, to obtain the corresponding desired range for the contact force between the surgical tool and tissue. Therefore, the two surgical scenarios are designed as shown in Table 2.

Table.2. Surgical scenarios

Surgical scenario	**1**	**2**
Surgical tasks	MVA	STC
Desired contact force (N)	2~3	>3~4
$\mathbf{f}_h$ during slave-heart contact (N)	3~4	
Force scaling factor	0.63	1

In simulations, both the human arm and the beating heart will be modeled mathematically. A harmonic function will be used to simulate the exogenous input force of the human arm, and produce a harmonic master-human interaction force with a maximum magnitude of ~ 4 N.

In the experiments, an actual human operator can actively maintain the master-human interaction force at any level. To clearly present the force tracking performance during contact, the operator is instructed to hold the surgical instrument against the tissue with 2 N of force for ~15s followed by 3-4 N for ~15s, and then with 2 N for ~15s.

It is worth noting that the desired contact forces for the two surgical scenarios should be examined in the direction normal to the tissue plane [37]. In the experimental user study, the motions of the robots contain 2 DOFs (degree of freedoms). Detailed information with regard to the user study is presented in Sec. 5.2.

4. Simulation Results

A teleoperation system is modeled and simulated in MATLAB/SIMULINK. In the simulations, two PHANToM Premium 1.5A robots with 3-DOF (shown in Fig. 3) are modeled to play the role of the master and slave robots. As the two tasks are single-DOF, only simulation along the *x*-axis of each PHANToM robot is presented.

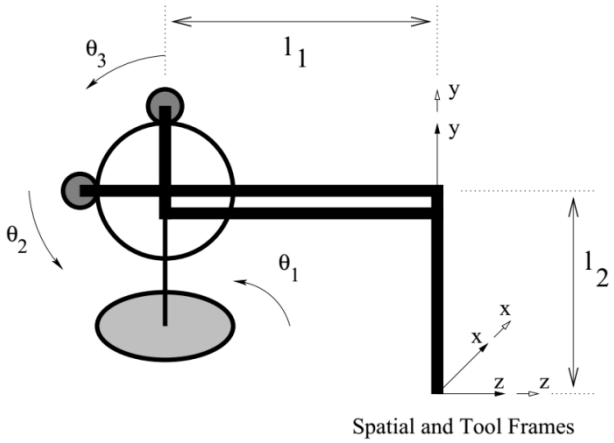

Fig.3. Zero configuration of PHANToM (adapted from [38]).

In terms of modeling, the experimentally identified transfer function model for the PHANToM at the center of the workspace along the *x*-axis is expressed as [38]

$$\frac{x}{f} = \frac{1}{s_2} \frac{s^2 + 5.716s + 9.201\times10^4}{3.329\times10^{-6}s^2 + 0.001226s + 1.536} \qquad (5)$$

It has been shown that this linear model closely approximates the low-frequency behavior (up to about 200 Hz) of the robot dynamics [38].

The interaction force between the master and the operator, $\mathbf{f}_h$, and the interaction force between the slave and the environment, $\mathbf{f}_e$, can be experimentally measured by force sensors. Alternatively, in simulations, $\mathbf{f}_h$ and $\mathbf{f}_e$ will be calculated based on the dynamic models for the operator and the beating heart, respectively. The dynamics are assumed to be the following two second-order LTI models [39], [40]:

$$\mathbf{f}_h = \mathbf{f}_h^* - (m_h\ddot{\mathbf{x}}_m + c_h\dot{\mathbf{x}}_m + k_h\mathbf{x}_m) \tag{6}$$

$$\mathbf{f}_e = m_e\ddot{\tilde{\mathbf{x}}}_s + c_e\dot{\tilde{\mathbf{x}}}_s + k_e\tilde{\mathbf{x}}_s \tag{7}$$

Here, $\mathbf{f}_h^*$ is the exogenous input force of the human operator generated by the muscles, and $\tilde{\mathbf{x}}_s = (\mathbf{x}_s - \mathbf{x}_e)$ is the relative displacement between the slave robot and the beating heart. m_h, m_e, c_h, c_e, k_h, k_e are the mass, damping, and stiffness parameters of the operator arm and the heart tissue, respectively.

The exogenous input force of the human operator and the oscillatory motion of the beating heart along the *x*-axis are simulated, respectively, as

$$f_h^* = 5 - 5\cos(0.05 - \pi t) \tag{8}$$

$$x_e = -0.005\cos(7.5t) + 0.005 \tag{9}$$

The parameters of the operator and the heart models, based on [35], [41], are shown in Table 3. Based on the adjustment guidelines presented in Sec. 2.5 and the scaling factors for the position and force described in Sec. 3, the parameters of the master and slave impedance models for contact and noncontact cases are shown in Table 3. The PID controllers for the master and slave robots used in simulations are the same for both robots. The parameters of the controllers are chosen to be K_p= 125, K_i= 9.21, K_d= 0.0103.

It should be mentioned that in simulations, as there is no force sensor to directly measure the contact force, contact will be detected based on position. To simulate the cases of non-contact and contact, the heart position was set to have an offset from the initial position of the slave robot. Once the position of the slave exceeded this offset, contact occurred. Based on this, each trial was divided into three steps: approach the heart, make contact with the heart, and break contact with the heart. The first and third phases belong to the noncontact case. Additionally, to further simulate the realistic force sensor noise, the calculated force signals were corrupted by an additive zero-mean Gaussian noise with variance of 0.005 N.

For the first scenario, the mean absolute errors (MAEs) of the master and the slave positions with respect to their corresponding reference positions calculated from (1) and (2) were 8.25×10^{-10} m and 2.76×10^{-8} m, respectively. For the second scenario, the MAEs between the real positions of the robots and their reference positions were 8.32×10^{-10} m and 3.40×10^{-8} m, respectively. These demonstrate the designed controllers achieved position tracking successfully.

Table.3. Model parametes of the human operator's arm, the beating heart, the master robot and the slave robot

Parameters	**Human Operator**	**Beating Heart**	**Noncontact**		**Contact**	
			Master Z_{m1}	**Slave** Z_{s1}	**Master** Z_{m2}	**Slave** Z_{m2}
Stiffness (N/m)	k_h = 300	k_e = 200	k_{m1} = 10	k_{s1} = 10	k_{m2} = 200	k_{s2} = 10
Mass (kg)	m_h = 3.25	m_e = 0.25	m_{m1} = 10	m_{s1} = 10	m_{m2} = 200	m_{s2} = 0.004
Damping (Ns/m)	c_h = 20	c_e = 4.5	c_{m1} = 14	c_{s1} = 14	c_{m2} = 280	c_{s2} = 0.28

Fig. 4 shows the positions of the master and slave robots for the two surgical scenarios. It can be seen that when the slave robot was near the heart, the non-contact and contact cases alternatively occurred because of the movement of the heart. To reduce the number of repetitive switching, when the slave robot was near the heart, both the impedances of the master and slave models were increased continuously from $Z_{m1}(Z_{s1})$ to Z_{m2}. If the scaled human-master interaction force were greater than the slave-heart interaction force, based on model (2) the switch would stop. Otherwise, the slave robot would be pushed back, and repetitive switching would go on. In Fig. 4, for both scenarios, switching appeared during the transitions between contact case and non-contact case. However, large force scaling factor resulted in large human-master interaction force, which leaded to less switching and small motion amplitude of the master robot. The zoomed up transitions clearly showed that the contacts between the slave robot and the heart were weak.

For the sake of following calculations, the contact period was defined as the slave robot made firm contact with the heart, that is, no switching occurred during the contact period. The rest periods were treated as non-contact case.

During non-contact periods, the position tracking MAEs between the slave robot and the master robot for the two scenarios were 2.64×10^{-4} m and 1.31×10^{-4} m, respectively.

When the slave robot made contact with the heart, to obtain the dominant frequencies associated with the heartbeat and human arm's motions, a fast Fourier transform (FFT) with a

Hamming window was applied to the slave robot position. In Fig. 4 (a), the high-frequency component of the slave robot position (HFCS) had amplitude of 4.67 mm that was 93.4% of the beating heart's motion amplitude (5mm). The low-frequency component of the slave robot position (LFCS) had an amplitude of 3.92 mm, that was 109% of the scaled amplitude of the human operator motion (note that $k_f x_m = 3.58$ mm). The results for the other scenario incorporating the first one were summarized in Table 4.

Table.4. Position-tracking results in simulations

Surgical scenario		**1**	**2**
High frequency amplitude	HFCS (mm)	4.67	4.76
	Heart motion (mm)	5	5
	Ratio	93.4%	95.2%
Low frequency amplitude	LFCS (mm)	3.92	7.75
	Scaled human motion (mm)	3.58	7.26
	Ratio	109%	107%

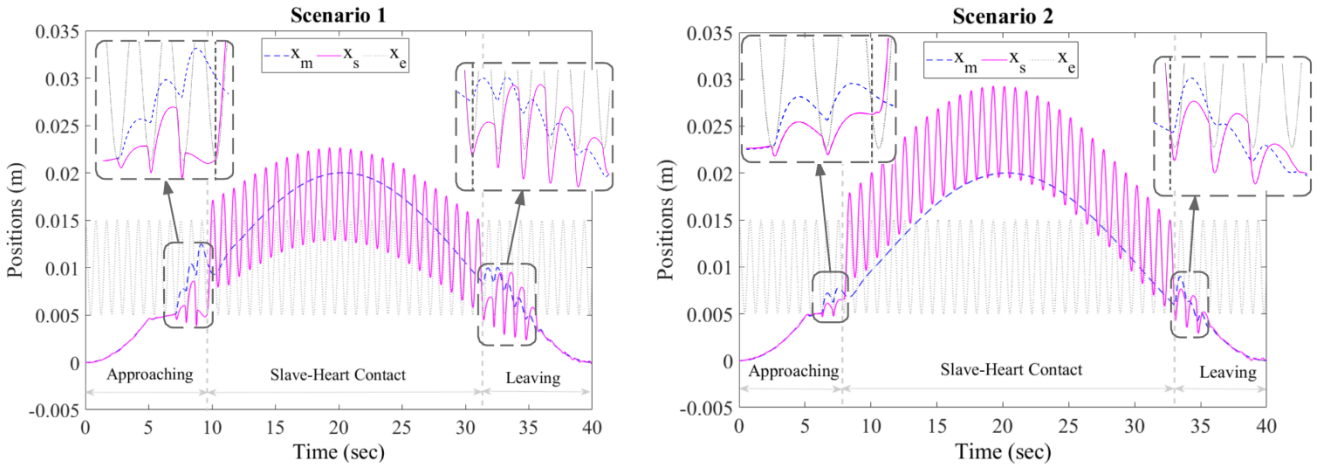

(a) (b)

Fig. 4. Simulated position-tracking performance. The positions of the master and slave robots for surgical scenario amenable to task: (a) mitral valve annuloplasty, and (b) soft tissue cutting. The dashed blue line and the solid pink line denote the real positions of the master and slave robots, respectively. The trajectory of the heart tissue is presented by the dotted gray line.

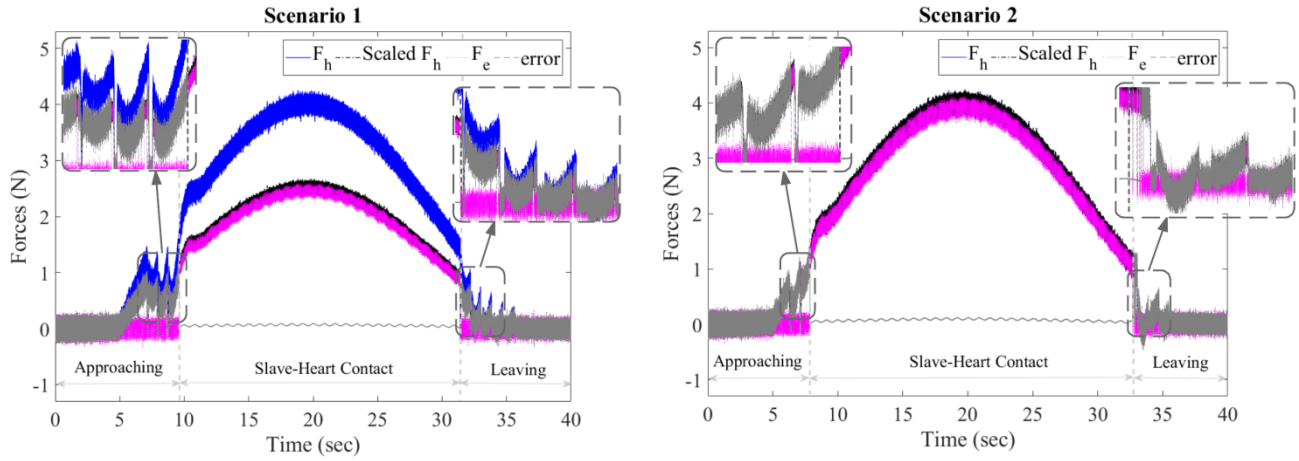

(a) (b)

Fig. 5. The simulated human-master interaction force (solid blue line) plotted versus the simulated slave-heart interaction force (dotted pink line) for surgical scenario amenable to task: (a) mitral valve annuloplasty, and (b) soft tissue cutting. In addition, the scaled-down human-master

contact forces (dash-dotted black line) and force errors between the scaled human-master interaction force and the slave-heart interaction force (dashed black line) are presented as well.

The MAEs between the slave robot position and the summation of the scaled master robot position and the beating heart position for two tasks were 1.73 mm, and 1.17 mm, respectively, which are satisfactorily small given that the main criteria for task success were defined in terms of applying the required force levels on tissue.

Fig. 5 shows the force performance. The scaled human-master interaction forces were approximately equal to the slave-heart interaction forces with MAEs between them of 0.12 N, and 0.15 N during contact period for the two surgical scenarios, respectively. Moreover, the zoomed up transitions between contact and non-contact cases show that the contact for scenario 1 is weaker than that for scenario 2. It is because small force scaling factor leads to small scaled human-master interaction force. If this force were smaller than the slave-heart interaction force, the slave robot would be rebounded.

5. Experimental Results

Following the successful simulation study, experiments are performed with a teleoperated robotic system. The experimental setup employs a 3-DOF Phantom Premium 1.5A robot (Geomagic Inc., Wilmington, MA, USA) as the master robot and a 2-DOF Quanser planar robot (Quanser Consulting Inc., Markham, ON, Canada) as the slave robot (Fig. 6). To measure the applied interaction forces of the human operator and the heart tissue, the Phantom Premium and Quanser robots are respectively equipped with a 6-axis 50M31 force/torque sensor (JR3 Inc., Woodland, CA, USA) and a 6-axis Gamma force/torque sensor (ATI Industrial Automation, Apex, NC, USA), respectively. The beating heart is simulated by an artificial plastisol-based tissue attached to a custom-built mechanical cam which produces peak-to-peak amplitude of 9 mm and has a fundamental frequency of 64 bpm (1.07 Hz) to simulate the beating-heart's motion which temporally matched to an ECG signal [14]. To simplify the analysis, the motion direction of the heart simulator is adjusted to be the same as the x direction of the robots. As mentioned before, the positions and forces presented in Sec. 5.1 (1-DOF scenarios corresponding to the surgical tasks) are along the x direction, and in Sec. 5.2 (2-DOF user study) are along x and y directions.

Unlike the simulations, in the experiments the stiffness of the heart tissue is unknown, so the impedance parameters for the master robot during contact are arbitrarily set to be k_{m2}= 300 N/m, m_{m2}= 300 kg, and c_{m2}= 420 Ns/m. The parameters for the slave impedance model during contact are set at k_{s2}= 50 N/m, m_{s2}= 0.02 kg, and c_{s2}= 1.4 Ns/m. The parameters of PID controllers for the master robot are K_{p_m} = 1000, K_{i_m} = 200, K_{d_m} = 1. The PID controller parameters for the slave robot are K_{p_s} = 1000, K_{i_s} = 0, K_{d_s} = 20. Note that the master and slave robots are not identical in the experiments as they were in the simulations.

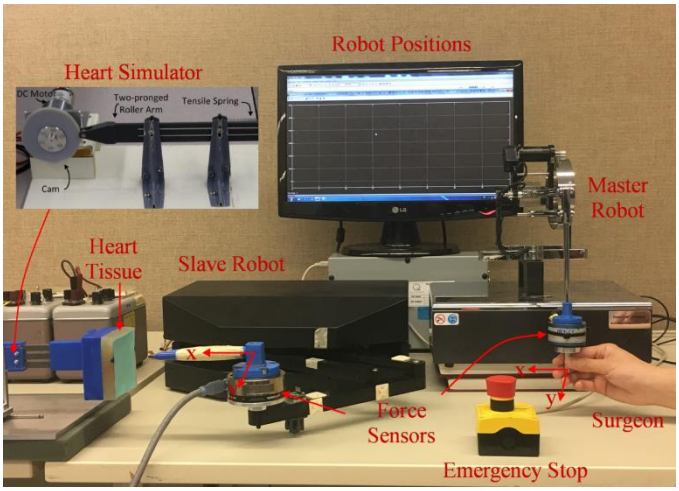

Fig. 6. Experimental setup: master robot, slave robot and beating heart simulator.

5.1. *Surgical scenarios validation*

Testing indicated that in the x direction, a threshold of 0.3 N for the slave-heart interaction force was appropriate to detect the contact state surgical tool and tissue. Based on this force threshold, each trial was divided into three steps as well: approach the heart, make contact with the heart, and break contact with the heart.

The position-tracking performances for two different surgical scenarios are shown in Fig. 7. The MAEs between the master robot position and its reference position generated by the impedance model (1) for two scenarios were 0.54 mm, and 0.44 mm, respectively. The MAEs between the slave robot position and its reference position generated by the impedance model (2) for the two surgical scenarios were 0.47 mm, and 0.64 mm, respectively. The above MAEs were calculated across the two phases of approaching, making contact with, and breaking contact with the heart.

In Fig. 7 (a), by applying FFT to the position data of the slave robot for contact case, the high-frequency component has an amplitude of 3.96 mm, which is 88% of the amplitude of the heart's motion (4.5 mm), and the amplitude of the low-frequency component was 2.37 mm, which was 75% of the scaled master motion amplitude (note that $k_f x_m$= 3.16 mm). Sec. 2.4 presented the slave robot would comply with the heart's motion and follow the theoretically scaled position of the master robot ($\mathbf{X}_s \rightarrow (k_f Z_{m2} / Z_e) \mathbf{X}_m + \mathbf{X}_e$). However, the

experimental results show that only 75% of $k_f x_m$ was transmitted to the slave robot, which means the ratio of Z_{m2}/Z_e was less than 1. In other words, the artificial tissue used in the experiments is more rigid than the stiffness of the master robot (300 N/m). More results about the two surgical scenarios are shown in Table 5.

In summary, the results in Fig. 7 demonstrate that (a) the local position controllers used in the system guarantee the robots follow their corresponding reference impedance positions, (b) when the slave robot is getting close to or is leaving the tissue, the master and slave robots have very similar positions, and most importantly (c) when the slave robot makes contact with the tissue, the slave robot successfully complies with the fast oscillatory motions of the tissue while following the (scaled) position of the master robot as closely as possible.

Table.5. Position-tracking results in expeiments

Surgical scenario		**1**	**2**
High frequency amplitude	HFCS (mm)	3.96	4.12
	Heart motion (mm)	4.5	4.5
	Ratio	88%	93.6%
Low frequency amplitude	LFCS (mm)	2.37	4.98
	Scaled human motion (mm)	3.16	6.07
	Ratio	75%	82%

In addition, the transitions between non-contact and contact are zoomed up in Fig. 7 as well. Similarly to the simulations, in order to obtain steady slave-tissue contact and avoid chattering during interaction, the human operator should exert relatively a large force to make the scaled-down human-master interaction force greater than the slave-heart interaction force. Once the slave-heart interaction force was kept greater than the force threshold 0.3 N, the switch would stop. The transitions shown in Fig. 7 for the two scenarios demonstrate that the larger the force scaling factor is the less the number of repetitive switching will be.

Fig. 8 demonstrates the performance of non-oscillatory haptic perception for each scenario. Based on the reference impedance model for the slave robot (2), when slave robot made contact with the tissue, the scaled-down human-master interaction force was transmitted to model (2). The MAEs between the scaled human-master interaction force and the slave-tissue interaction force for the two surgical scenarios were 0.33 N, and 0.36 N, respectively. The zoomed up parts in Fig. 8 demonstrate that large slave-heart contact force reduces the number of repetitive switching between contact and non-contact cases when the slave robot is near the heart.

These experimental results in Fig. 7 and Fig. 8 suggest that the proposed switched-impedance control based telerobotic system achieves position-tracking and non-oscillatory tactility simultaneously even when the slave is making contact with the beating heart. In addition, regarding the two specific scenarios, by choosing an appropriate force scaling factor, the ideal behaviors of position and force are achieved.

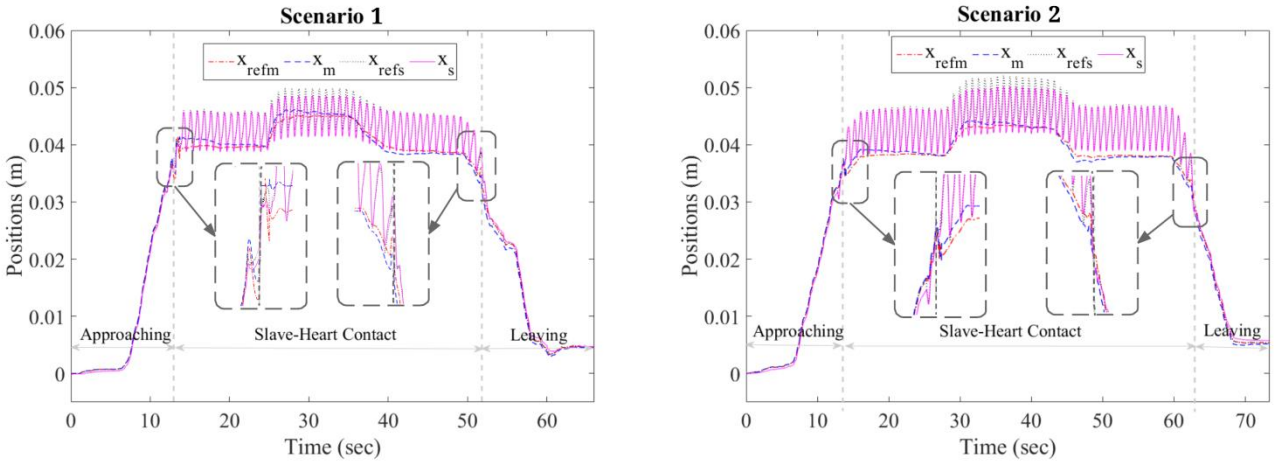

Fig. 7. Experimental position-tracking performance of the master and slave robots for surgical scenario amenable to task: (a) mitral valve annuloplasty, and (b) soft tissue cutting. The reference positions and the actual positions of the master and slave robots are presented. The dash-dotted red line and the dotted black line denote the reference positions of the master and slave robots, respectively. The dashed blue line and the solid pink line denote the actual positions of the master and slave robots, respectively.

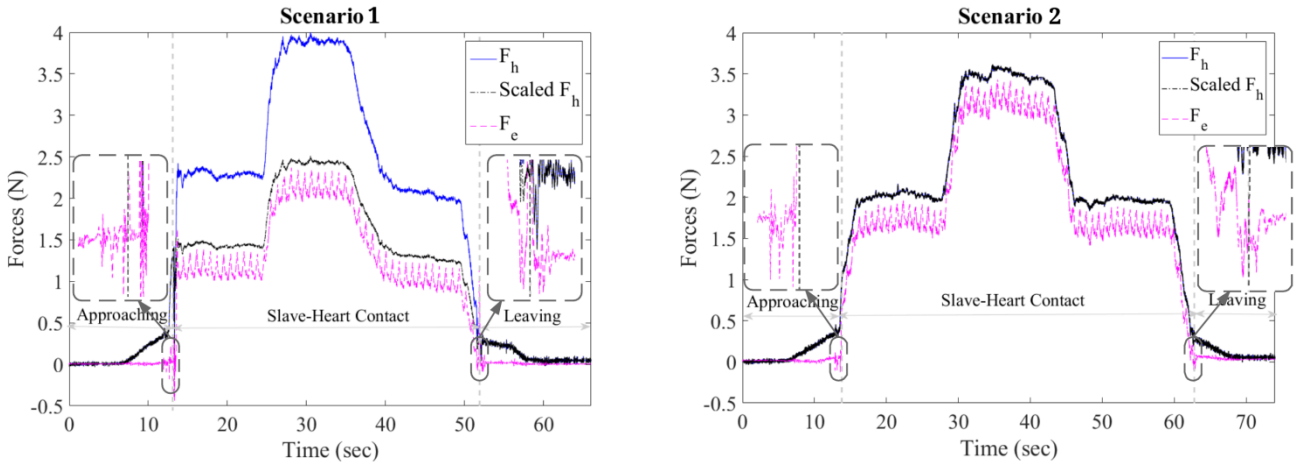

(a) (b)

Fig. 8. The experimental human-master interaction force (solid blue line) plotted versus the experimental slave-heart interaction force (dashed pink line) for surgical scenario amenable to task: (a) mitral valve annuloplasty, and (b) soft tissue cutting. The scaled human-master interaction forces (dash-dotted black line) are also presented.

5.2. *User study*

The experimental user study presented here was selected to emulate the motion requirements of cutting tissue. It involves drawing a line on the surface of the mock beating heart by using a marker mounted on the end of the slave robotic arm. This user study was approved by the University of Alberta's Research Ethics Office #Pro00055825.

In this study, the simulated heart is moving back and forth along the *x* direction. The participant commands the slave robot to approach the tissue surface by manipulating the master robot. After the slave robot makes contact with the tissue, the participant commands the slave robot to draw a solid legible line along the robot's *y* direction for ~ 3 cm. To record the results, for each trial a paper is stuck to the surface of the mechanical beating heart simulator (on top of the soft plastisol tissue to still recreate the soft heart tissue). The process requires a prolonged contact with the surface while the contact forces should not be too large to cause damage to the tissue. This task is completed with motion compensation (the proposed strategy) and without motion compensation (simple direct-force-reflection haptic teleoperation control).

The task included 5 participants (4 females and 1 male). The participants aged 20-30 and were graduate student volunteers. Each participant trained with and without motion compensation until he/she got used to the system. Then, 10 trials in which each participant alternated between with and without motion compensation cases were completed.

The results of line drawing time and break points number are listed in Table 6 with respect to the two cases (with and without motion compensation). To compare the results of the two cases, a paired two-sided *t-test* was used to obtain the probability of the null hypothesis for the 10 trials. Data are shown as means ± standard derivations. Means were considered significantly different if $P < 0.05$.

Table.6. Experimental results of time and break points

Motion Compensation	**Yes**	**No**	**P-value**
Drawing Time (s)	**18.67** ± 2.74	**25.20** ± 2.45	< 0.0001
Number of Break Points	**0.68** ± 0.90	**4.24** ± 1.83	< 0.0001

With motion compensation, the mean drawing time was 26% less than the time measured without motion compensation. The mean and standard deviation of the break points number were reduced sharply when providing motion compensation. The P-values indicate that there was a significant difference between providing and not providing compensation with respect to the drawing time and the number of break points.

In addition, considering all of the trials of the 5 participants, the means and standard deviations of the force by operator on master robot and the force by slave robot on tissue with and without compensation are shown in Table 7. Providing no compensation, the two standard deviations of forces were roughly 10 times and 2 times, respectively, greater than those measured when provided compensation. In addition, when there was no motion compensation provided, the human-master interaction forces were generally smaller than those provided compensation. It is because participants usually did not apply large forces to the master robot to avoid unexpected

tool-tissue collision. If the human-master contact force were too large, it was more likely to puncture the paper.

When there was no motion compensation provided, the user had to make compensation manually as well as attempted to draw a solid line along the perpendicular direction. It was not easy for the user to achieve the two objectives simultaneously. Fig. 9 shows the drawn lines without motion compensation, which include lots of break points. In Fig. 10, the robot positions and the interaction forces in both *x* and *y* directions are presented. It can be seen that in the *x* direction, the motion synchronization was difficult for the human operator to achieve and the slave-heart interaction force level was hard to control. In the *y* direction, both the positions and the forces have oscillatory motions with small amplitudes, which appeared due to tissue deformation and friction.

Table.7. Experimental results of forces

Motion Compensation	**Yes**	**No**
Force by Operator on Master in *x* direction (N)	1.84 ± **0.05**	1.57 ± **0.48**
Force by Slave on Tissue in *x* direction (N)	1.41 ± **0.22**	1.55 ± **0.53**

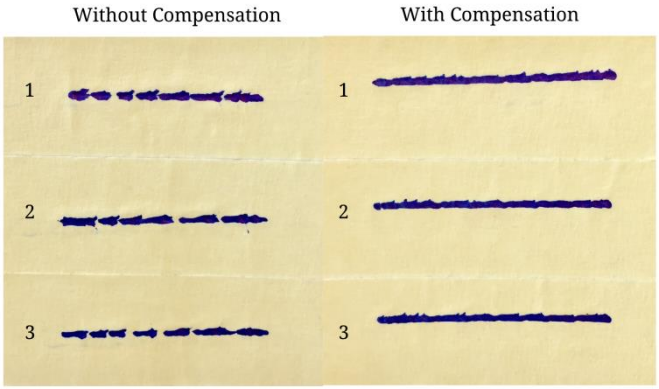

Fig. 9. Comparison of line results.

When motion compensation was provided, it was easier for the user to draw a solid line along the direction perpendicular to the movement direction. The lines shown in Fig. 9 with compensation demonstrate that the proposed method achieves better results. The positions of the master robot in both *x* and *y* directions do not include the oscillatory motions of the slave robot (Fig. 11). In the *x* direction, the slave robot successfully synchronizes its movement with the moving heart's motion, and the human-master interaction force provides the user a steady contact force. This steady force was simultaneously transmitted to the slave robot, which made the control of the slave-heart contact force easily. In the *y* direction, the positions and forces of the slave robot were both oscillatory due to unexpected tissue deformation and friction. Similarly, these oscillatory behaviors did not influence the frequencies of the positions and forces of the master robot.

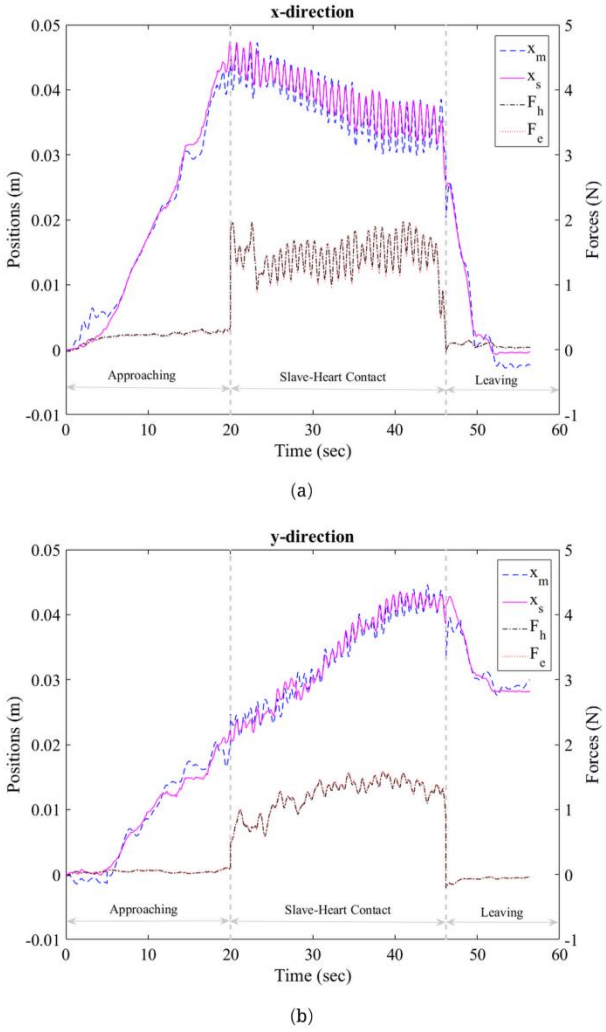

Fig. 10. Robot positions and interaction forces without motion compensation (a) in the *x* direction and (b) in the *y* direction. The dashed blue line is the position of the master robot. The solid pink line is the position of the slave robot. The dash-dotted black line shows the human-master interaction force. The dotted red line indicates the slave-heart interaction force.

6. Conclusion

This paper demonstrated the effectiveness of the proposed switched-impedance controlled master-slave teleoperation system, which is designed to both implement fast compensation for the beating heart's motion and apply accurate interaction force to the heart tissue to perform surgical

tasks on or inside the heart. The desired behavior was achieved in the proposed system by switching the parameters of two reference impedance models for the master and slave robots. When the slave robot does not make contact with the beating heart, the slave robot closely follows the motion commands of the human operator given to the master robot. *Once contact occurs, the slave robot complies with the combined motion of the master robot and the beating heart, and enables the human operator to perceive non-oscillatory interaction force that is akin to a sense of operating on a seemingly idle heart.* Results of both simulations and experiments for two surgical scenarios suggest that the proposed telerobotic system achieves the stated goals. In addition, the user study of line drawing demonstrates that the proposed switched impedance control strategy offers time-saving, perfect lines, and easy control of the slave-heart interaction force compared to the case without motion compensation.

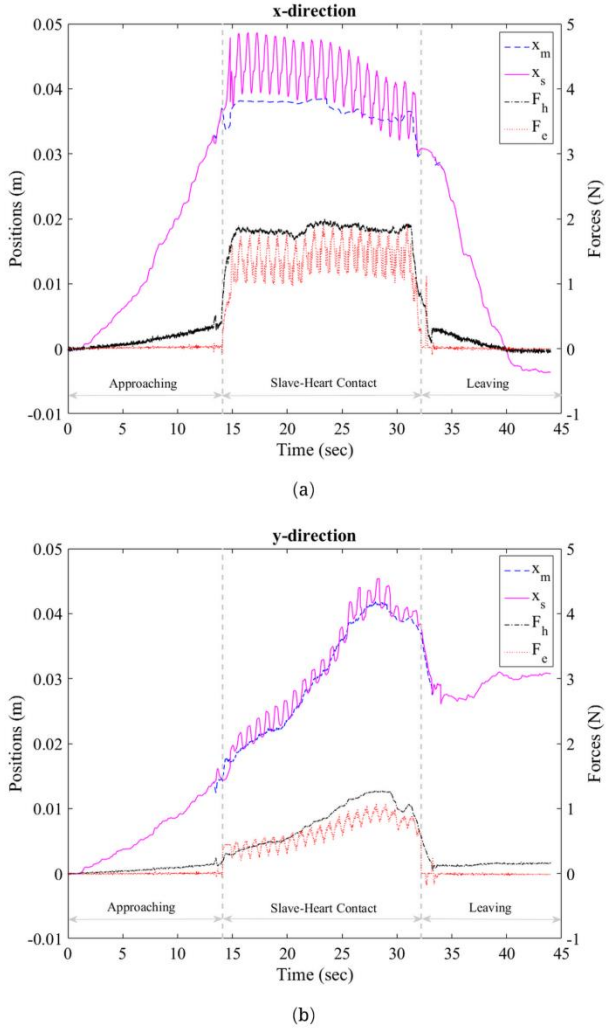

Fig. 11. Robot positions and interaction forces with motion compensation (a) in the *x* direction and (b) in the *y* direction. The dashed blue line is the position of the master robot. The solid pink line indicates the position of the slave robot. The dash-dotted black line is the human-master interaction force. The dotted red line shows the slave-heart interaction force.

Acknowledgments

This work is supported by the Canada Foundation for Innovation (CFI) under grant LOF 28241， the Alberta Innovation and Advanced Education Ministry under Small Equipment Grant RCP-12-021, the Natural Sciences and Engineering Research Council (NSERC) of Canada under grant RGPIN 372042, the Natural Sciences and Engineering Research Council (NSERC) of Canada under grant RGPIN 03907, and the China Scholarship Council (CSC) under grant [2015]08410152.

References

[1] D. Paparella, T. M. Yau, and E. Young, Cardiopulmonary Bypass Induced Inflammation: Pathophysiology and Treatment. An update, *Eur. J. Cardio-thoracic Surg.* **21**(2) (2002) 232-244.

[2] D. C. Bellinger, D. Wypij, K. C. K. Kuban, L. A. Rappaport, P. R. Hickey, G. Wernovsky, R. A. Jonas, and J. W. Newburger, Developmental and Neurological sStatus of Children at 4 Years of Age After Heart Surgery With Hypothermic Circulatory Arrest or Low-Flow Cardiopulmonary Bypass, *Circulation* **100**(5) (1999) 526-533.

[3] J. Zeitlhofer, S. Asenbaum, C. Spiss, A. Wimmer, N. Mayr, E. Wolner, and L. Deecke, Central Nervous System Function After Cardiopulmonary Bypass, *Eur. Heart J.* **14**(7) (1993) 885-890.

[4] E. E. Tuna, J. H. Karimov, T. Liu, Ö. Bebek, K. Fukamachi, and M. C. Çavuşoğlu, Towards Active Tracking of Beating Heart Motion in the Presence of Arrhythmia for Robotic Assisted Beating Heart Surgery, *PLoS One* **9**(7) (2014) e102877(1-8).

[5] E. E. Tuna, T. J. Franke, O. Bebek, A. Shiose, K. Fukamachi, and M. C. Cavuşoğlu, Heart Motion Prediction Based on Adaptive Estimation Algorithms for Robotic Assisted Beating Heart Surgery, *IEEE Trans. Robot.* **29**(1) (2013) 261-276.

[6] Ö. Bebek and M. C. Çavusoglu, Intelligent Control Algorithms for Robotic-Assisted Beating Heart Surgery, *IEEE Trans. Robot.* **23**(3) (2007) 468-480.

[7] C. Riviere, J. Gangloff, and M. De Mathelin, Robotic Compensation of Biological Motion to Enhance Surgical Accuracy, *Proc. - IEEE*, **94**(9) (2006) 1705-1716.

[8] R. Ginhoux, J. Gangloff, M. de Mathelin, L. Soler, M. M. Arenas Sanchez, and J. Marescaux, Active Filtering of Physiological Motion in Robotized Surgery Using Predictive Control, *IEEE Trans. Robot.*, **21**(1) (2005) 67-79.

[9] S. B. Kesner and R. D. Howe, Position Control of Motion Compensation Cardiac Catheters, *IEEE Trans. Robot.* **27**(6) (2011) 1045-1055.

[10] S. G. Yuen, S. B. Kesner, N. V Vasilyev, P. J. Del Nido, and D.

Howe, 3D Ultrasound-Guided Motion Compensation System for Beating Heart Mitral Valve Repair, *Med. Image Comput. Comput. Interv.* **11**(1) (2008) 711-719.

[11] S. G. Yuen, D. T. Kettler, P. M. Novotny, R. D. Plowes, and R. D. Howe, Robotic Motion Compensation for Beating Heart Intracardiac Surgery, *Int. J. Rob. Res.* **28**(10) (2009) 1355-1372.

[12] P. Thienphrapa, A. Popovic, and R. H. Taylor, Guidance of a High Dexterity Robot under 3D Ultrasound for Minimally Invasive Retrieval of Foreign Bodies from a Beating Heart, in *IEEE Int. Conf. on Robotics and Automation* (Hong Kong 2014) 4869-4874.

[13] M. Bowthorpe and M. Tavakoli, Ultrasound-Based Image Guidance and Motion Compensating Control for Robot-Assisted Beating-Heart Surgery, *J. Med. Robot. Res.* **1**(1) (2016), 1640002(1-11).

[14] M. Bowthorpe, V. Castonguay-Siu, M. Tavakoli, Development of a Robotic System to Enable Beating-heart Surgery, *J. Robot. Society Japan* **32**(4) (2014) 23-30.

[15] M. Bowthorpe, M. Tavakoli, H. Becher, and R. Howe, Smith Predictor-Based Robot Control for Ultrasound-Guided Teleoperated Beating-Heart Surgery, *IEEE J. Biomed. Heal. Informatics* **18**(1) (2014) 157–166.

[16] M. Bowthorpe and M. Tavakoli, Generalized Predictive Control of a Surgical Robot for Beating-Heart Surgery Under Delayed and Slowly-Sampled Ultrasound Image Data, *IEEE Robot. Autom. Lett.* **1**(2) (2016) 892–899.

[17] M. Bowthorpe and M. Tavakoli, Physiological Organ Motion Prediction and Compensation Based on Multirate, Delayed, and Unregistered Measurements in Robot-Assisted Surgery and Therapy, *IEEE/ASME Trans. Mechatronics* **21**(2) (2016) 900-911.

[18] C. R. Wagner, N. Stylopoulos, P. G. Jackson, and R. D. Howe, The Benefit of Force Feedback in Surgery: Examination of Blunt Dissection, *Presence Teleoperators Virtual Environ.* **16**(3) (2007) 252-262.

[19] S. G. Yuen, N. V Vasilyev, J. Pedro, and R. D. Howe, Robotic Tissue Tracking for Beating Heart Mitral Valve Surgery, *Med. Image Anal.* **17**(8) (2013) 1236-1242.

[20] T. Chanthasopeephan, K. Mongkut, and T. Thonburi, Study of Soft Tissue Cutting Forces and Cutting Speeds, *Stud. Health Technol. Inform.* **98** (2004) 56-62.

[21] Z. Hu, W. Sun, and B. Zhang, Characterization of Aortic Tissue Cutting Process: Experimental Investigation Using Porcine Ascending Aorta, *J. Mech. Behav. Biomed. Mater.* **18** (2013) 81-89.

[22] O. Bebek and M. C. Cavusoglu, Model Based Control Algorithms for Robotic Assisted Beating Heart Surgery, in *Proc. IEEE Int. Conf. on Medicine and Biology Society* (New York, 2006) 823-828.

[23] S. B. Kesner and R. D. Howe, Robotic Catheter Cardiac Ablation Combining Ultrasound Guidance and Force Control, *Int. J. Rob. Res.* **33**(4) (2014) 631-644.

[24] S. B. Kesner, S. Member, R. D. Howe, and S. Member, Force Control of Flexible Catheter Robots for Beating Heart Surgery, in *Proc. IEEE Int. Conf. on Robotics and Automation* (Shanghai, 2011) 1589-1594.

[25] S. G. Yuen, D. P. Perrin, N. V Vasilyev, P. J. Nido, R. D. Howe, and S. Member, Force Tracking With Feed-Forward Motion Estimation for Beating Heart Surgery, *IEEE Trans. Robot.* **26**(5) (2010) 888-896.

[26] Y. Nakajima, T. Nozaki, and K. Ohnishi, Heartbeat Synchronization With Haptic Feedback for Telesurgical Robot, *IEEE Trans. Ind. Electron.* **61**(7) (2014) 3753-3764.

[27] M. Joinié-Maurin, B. Bayle, and J. Gangloff, Force Feedback Teleoperation With Periodical Disturbance Compensation, *Proc. IEEE Int. Conf. Robot. Autom.* (2011) 4828-4833.

[28] P. Moreira, C. Liu, N. Zemiti, and P. Poignet, Beating Heart Motion Compensation Using Active Observers and Disturbance Estimation, in *IFAC Symposium on Robot Control Int. Federation of Automatic Control* (Dubrovnlk, 2012) 741-746.

[29] P. Moreira, N. Zemiti, C. Liu, and P. Poignet, Viscoelastic Model Based Force Control for Soft Tissue Interaction and Its Application in Physiological Motion Compensation, *Comput. Methods Programs Biomed.* **116**(2) (2014) 52-67.

[30] M. Dominici and R. Cortesão, Cascade Robot Force Control Architecture for Autonomous Beating Heart Motion Compensation with Model Predictive Control and Active Observer, in *IEEE RAS & EMBS Int. Conf. on Biomedical Robotics and Biomechatronics* (Sao Paulo, 2014) 745-751.

[31] M. Dominici and R. Cortesão, Model Predictive Control Architectures with Force Feedback for Robotic-Assisted Beating Heart Surgery, in *IEEE Int. Conf. on Robotics and Automation* (Hong Kong 2014) 2276-2282.

[32] R. Cortesão and M. Dominici, Robot Force Control on a Beating Heart, *IEEE/ASME Trans. Mechatronics* **22**(4) (2017) 1736-1743.

[33] P. J. Berkelman, L. L. Whitcomb, R. H. Taylor, and P. Jensen, A Miniature Microsurgical Instrument Tip Force Sensor for Enhanced Force Feedback During Robot-Assisted Manipulation, *IEEE Trans. Robot. Autom.*, **19**(5) (2003) 917-922.

[34] K. J. Kuchenbecker and G. Niemeyer, Induced Master Motion in Force-Reflecting Teleoperation, *J. Dyn. Syst. Meas. Control* **128**(4) (2006) 800-810.

[35] C. R. Wagner, D. P. Perrin, R. D. Howe, N. Vasilyev, and P. J. Nido, Force Feedback in a Three-Dimensional Ultrasound-Guided Surgical Task, in *Proc. 14th Symp. Haptic Interfaces for Virtual Environment and Teleoperator Systems* (Alexandria, 2006) 43-48.

[36] S. B. Kesner and R. D. Howe, Discriminating Tissue Stiffness with a Haptic Catheter : Feeling the Inside of the Beating Heart, in *IEEE World Haptics Conference* (Istanbul, 2011) 13-18.

[37] D. T. Kettler, R. D. Plowes, P. M. Novotny, N. V. Vasilyev, P. J. Del Nido, and R. D. Howe, An Active Motion Compensation Instrument for Beating Heart Mitral Valve Surgery, in *Proc. IEEE/RSJ Int. Conf. on Intelligent Robots and Systems* (San

Diego, 2007) 1290-1295.

[38] M. C. Çavusoglu, D. Feygin, and F. Tendick, A Critical Study of the Mechanical and Electrical Properties of the PHANToM Haptic Interface and Improvements for High Performance Control, *Presence* **11**(5) (2002) 555-568.

[39] X. Liu and M. Tavakoli, Adaptive Inverse Dynamics Four-Channel Control of Uncertain Nonlinear Teleoperation Systems, *Adv. Robot.* **25**(13–14) (2011) 1729-1750.

[40] M. Sharifi, S. Behzadipour, and H. Salarieh, Nonlinear Bilateral Adaptive Impedance Control with Applications in Telesurgery and Telerehabilitation, *J. Dyn. Syst. Meas. Control* **138**(11) (2016) 111010(1-16).

[41] D. D. Matthew and M. Tavakoli, Measuring the Dynamic Impedance of the Human Arm Without a Force Sensor, in *Proc. IEEE Int. Conf. on Rehabilitation Robotics*, (Seattle, 2013).